LA-5615-MS

Informal Report

UC-34
Reporting Date: April 1974
Issued: May 1974

Design Considerations for a High-Pressure, Equation-of-State Experiment

by

Charles E. Ragan III

los alamos
scientific laboratory
of the University of California
LOS ALAMOS, NEW MEXICO 87544

UNITED STATES
ATOMIC ENERGY COMMISSION
CONTRACT W-7405-ENG. 36

In the interest of prompt distribution, this LAMS report was not edited by the Technical Information staff.

Printed in the United States of America. Available from
National Technical Information Service
U. S. Department of Commerce
5285 Port Royal Road
Springfield, Virginia 22151
Price: Printed Copy $4.00; Microfiche $1.45

DESIGN CONSIDERATIONS FOR A HIGH-PRESSURE, EQUATION-OF-STATE EXPERIMENT

by

Charles E. Ragan III

ABSTRACT

Experiments to measure shock velocity and particle velocity at pressures of ∿ 0.8 TPa and ∿ 2.1 TPa were fielded on an event at the Nevada Test Site. A description of the calculations involved in designing the experiment is presented. An underground nuclear explosion was used to produce a large flux of neutrons that were used to rapidly heat a slab of fissionable material. This material then drove a shock into a slab of molybdenum, which was chosen as a standard against which other materials could be calibrated. Basically the shock velocity measurements involved a determination of the transit time of the shock between points known distances apart. The particle velocity measurements involved a determination of the Doppler shift of low-energy neutron resonances for material behind the shock. This measurement was accomplished using time-of-flight (TOF) techniques with low-energy neutrons produced in a moderating material. The basic calculations needed for the design are: (1) Calculations of the neutron transport from the device to the driver material; (2) calculations of the shock strength due to fission heating and its subsequent time history in the shocked material; (3) calculations of the time history of the low-energy neutron flux; (4) calculations of the Doppler broadening and shifts of the neutron resonances.

Preshot calculations of the expected TOF signal for the two experiments are presented. A short discussion of the shot data is also presented. Both the shock velocity and the particle velocity measurements failed to work as expected. In the shock velocity measurement the background was as large as the signal itself, and in the particle velocity measurement a large background and neutrons from an unexpected source obscured the signal. These errors should be easy to correct, and the design considerations presented here should, for the most part, be valid for the next experiment.

I. INTRODUCTION

The high-pressure experiments on a shot at the Nevada Test Site (NTS) were designed to generate quite large shocks in some standard material and to measure both the shock velocity U_s and the mass or particle velocity U_p behind the shock. The parameters U_s and U_p are related through conservation relations[1] to the pressure P, specific volume V (= $1/\rho$), and specific internal energy E on both sides of the shock. The usual form of the energy conservation relation known as the Hugoniot equation is

$$E - E_o = 1/2\ (P + P_o)\ (V_o - V) \quad ,$$

where the subscript zero refers to the conditions ahead of the shock. Thus, a set of measurements of U_s and U_p leads through conservation equations to a determination of the part of the P, V, E equation of state (EOS) along the Hugoniot.

The shock velocity is, in principle, a readily measurable quantity and involves only a determination of the transit time of a shock between two points a known distance apart. Measurement of the particle velocity, however, is more difficult. At rather low pressures the particle velocity can be approximated by one half the free surface velocity -- a quantity which is not nearly as difficult to measure. At high pressures this is no longer true, but at extremely high pressure (tens of TPa), the Thomas-Fermi model of the atom can be used to calculate the pressure as

a function of the specific volume, which can be related to U_s as a function of U_p. Several Russian experimenters[2-6] have assumed that this theoretical calculation at extremely high pressure could be extrapolated downward in pressure to meet the existing data, in the case of lead, at approximately 1.0 TPa. Then, with lead as a standard, they used simultaneous measurements of the shock velocity in iron and in lead to determine an EOS point on the iron Hugoniot at 5.0 TPa. They also did similar experiments to determine EOS Hugoniot points for copper, cadmium, water, and quartz.

The main uncertainty in the above experiments lies in the extrapolation of the lead Hugoniot down from high pressures. A determination of several high-pressure points on the Hugoniot for one material would allow it to be used as a standard without requiring a theoretical extrapolation. Then experiments similar to those of the Russians could be based on a more sound experimental standard.

Particle velocities for shock pressures in the region of 2.0 TPa are about 10 mm/μs. If a neutron beam is passed through the material in the direction of the shock motion, then the material behind the shock will see effectively lower energy neutrons than would stationary material, and a given neutron resonance in the material behind the shock will remove neutrons of higher energy than if the material were stationary. Thus the position of a resonance observed by a stationary detector will be shifted up in energy, and the amount of the shift will be related to the particle velocity. (This, of course, assumes uniform motion in the material behind the shock front.)

With these considerations in mind, a search was made for a material to be used as a standard, one of the main additional requirements being that it have a rather high boiling point in order not to be easily vaporized by the neutrons which were to be used to generate the shock. Lead was ruled out because of its anomalously low density and because of its low boiling temperature. Another requirement of the standard was that it not have many low-energy (< 500 eV) neutron resonances in the cross section. This consideration ruled out tungsten and tantalum. The best choice of material, with these restrictions, appeared to be molybdenum, and when theoretical considerations indicated that molybdenum was a material whose EOS could be calculated rather accurately, it was chosen for the standard.

Experimental data[7] for U_s vs U_p have been obtained up to a pressure of $\sim$ 0.2 TPa for molybdenum, and using new laboratory techniques[8] these data can be extended up to a pressure of about 0.7 TPa. Since the method of measuring the particle velocity by observing the Doppler shift of neutron resonances is new, there is the possibility of systematic errors inherent in the process which have not been considered. Therefore, it was decided that a data point at a pressure that could approximately be obtained in the laboratory would be useful. Thus, two experiments were fielded on an underground shot at NTS, one at a pressure of approximately 0.8 TPa and one at a pressure of 2.1 TPa. These pressures would allow an accuracy of $\pm$ 2% in the U_p measurements to be obtained[9] and were chosen because they provided two rather different molybdenum preheat temperatures and Doppler shifts.

With these basic problems somewhat decided, it remained to design the detailed material configuration for generating the shock and for producing the required low-energy neutrons used to observe the Doppler shifts of the resonances. Since neutrons were required for observing the resonance shifts, one method of generating the shock would be by "instantaneous" neutron-induced fission heating of some fissionable drive material, with subsequent transmission of the shock into an adjacent slab of molybdenum. The only way to obtain the required large neutron flux would be from an underground nuclear explosion. If the neutron resonances in the molybdenum itself were used to determine the particle velocity, then the measurement would be averaged over all the material behind the shock. However, if a thin foil of some other material which would move at the same speed as the molybdenum were used, then the measurement would be localized with the only uncertainty being how closely the foil velocity matched the molybdenum velocity. (Hydrodynamic calculations indicate that for foils about 0.1-mm thick the velocities should be well matched.)

The basic calculations needed for the design were thus fourfold.

(1) A calculation of the neutron transport from the nuclear device to the fissionable driver and the resulting fission heating of the driver and the molybdenum preheat.

(2) A calculation of the shock strength due to the fission heating and its time history in both the driver and the molybdenum. (The latter, of course, requires just that information that is being sought: the shock behavior in molybdenum.)

(3) A calculation of the time history of the low-energy neutron flux from some moderating material placed either below the driver or between the driver and molybdenum.

(4) Calculations of the resonance shapes and shifts for both the molybdenum and the indicator foil.

Calculations 1 and 3 were carried out using MCNG -- a neutron-gamma ray Monte Carlo code.[10] The calculations of 2, based on the output from 1, were performed using the code PAD[11] of the LASL EOS group. The calculations of 4 were carried out using a code to be described in Sec. II-D.

II. CALCULATIONAL DETAILS AND RESULTS

A. Monte Carlo Calculations of Neutron Transport and Heating

These calculations can be divided into four parts: (1) Those using a monoenergetic 14-MeV source, (2) those using a "fission" spectrum neutron source, (3) those using OyH_3 instead of oralloy to drive the shock into the molybdenum, and (4) those done to ensure uniform heating across the driver surface. (The symbol Oy stands for oralloy which is composed of 93.5% ^{235}U and 6.5% ^{238}U.) Similar geometry was used for parts 1 through 3. This geometry, using 24 cells in MCNG, is shown in Fig. 1. The cross sections used were the standard ones in the MCNG library, except for those for ^{235}U and ^{238}U. These cross sections were obtained by Doppler-broadening the ENDF-B cross sections to a temperature of 50 eV, the expected temperature of the fission-heated oralloy.

The two important factors in these calculations are the rate of energy deposition in the driver and the ratio of the total energy deposited in the driver to that deposited in the molybdenum. The larger this ratio, the better the conditions ahead of the shock approximate ambient conditions (i.e., molybdenum at room temperature). The output from MCNG is heating or energy deposited in units of TeV/m^3 per source neutron for any cell requested. Thus for a given number of source neutrons, the energy deposited per gram in the driver could be

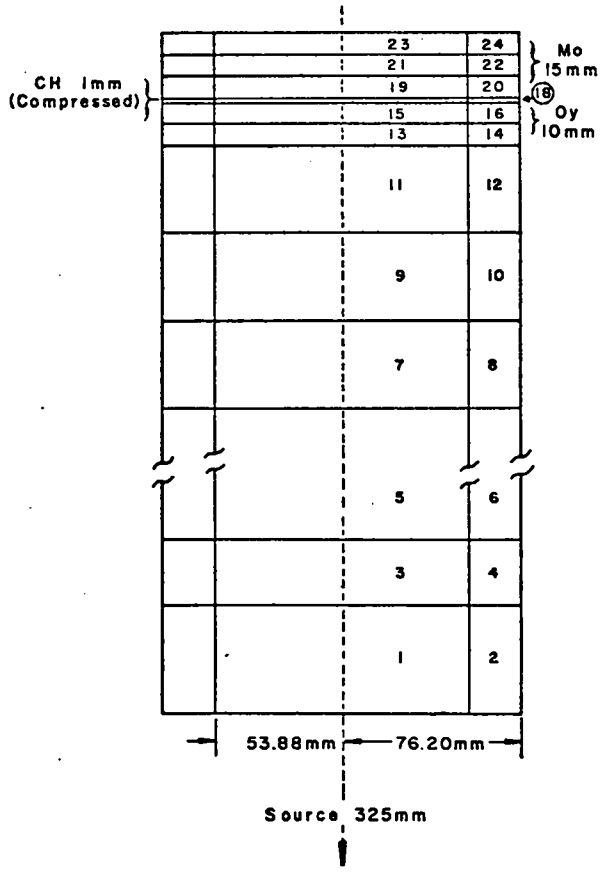

Fig. 1. Drawing of the cell geometry used in the Monte Carlo code MCNG. For most of the calculations, this 24-cell cylindrical geometry was used with the neutrons biased to start in the cone subtended by the oralloy. In order to reduce the neutron fluence, cells 1 and 2 were filled with $(CH_2)_n$ and cells 3 and 4 were filled with lead. Cells 5 and 6 were left void, while the contents of cells 7-12 were varied from run to run in order to optimize the ratio of the energy deposited in the oralloy to that deposited in the molybdenum. The oralloy was placed at a distance of 750 mm from the source and the cell thicknesses were varied from run to run. The uniformity of heating was determined by comparing the energy deposited in cells 13 and 14 and in cells 15 and 16.

determined. There are two contributions to the molybdenum heating: (1) that due to neutron interaction through both elastic and nonelastic events, and (2) that due to the absorption of gamma rays. The early runs done with MCNG contained no gamma-ray production cross sections for the molybdenum; therefore, all the inelastic events were assumed to

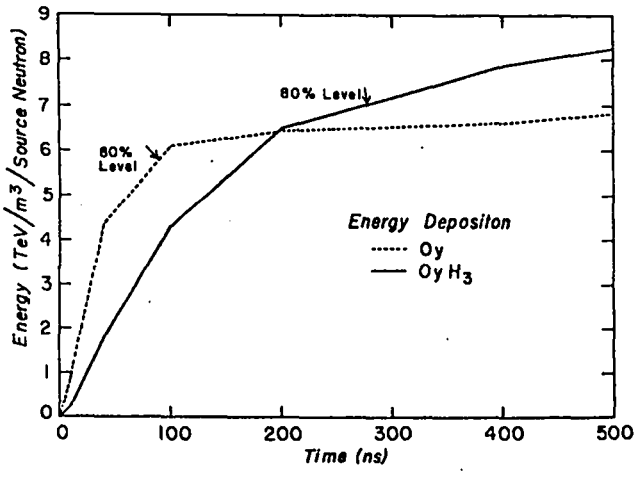

Fig. 2. Plot of the total energy deposited in the oralloy and OyH_3 drivers as a function of time. The heating pulse is much slower in OyH_3 and does not reach the 80% level until approximately 290 ns. These heating rates were calculated using the Monte Carlo code MCNG. The heating is in units of TeV/m^3 per source neutron.

deposit the total gamma-ray energy in the molybdenum. Later calculations with gamma-ray production cross sections for the molybdenum indicated that about two-thirds of the gamma-ray energy produced in the molybdenum was absorbed. The main mechanism for energy deposition in the driver material was fission heating, with gamma heating contributing less than 5%.

The ratio of the heating in the driver to that in the molybdenum ranged from 50 to 200. The smallest ratio was obtained with the OyH_3 driver. However, this is misleading since less energy deposition in OyH_3 is needed to drive a given shock into the molybdenum than for an oralloy driver. This effect results from a better impedance match between the OyH_3 and the molybdenum. The real drawback of the OyH_3 is the fact that the heating occurs relatively slowly. Since the cross section for ^{235}U is large for low-energy neutrons, the neutrons moderated by the hydrogen produce fission heating at times $>> 0.20$ μs after the initial burst. This causes the shock into the molybdenum to have a rather slow rise. Figure 2 shows a plot of the energy deposited in oralloy and OyH_3 drivers as a function of time.

For incident 14-MeV neutrons, the ratio of the specific energy deposited in the oralloy to that in the molybdenum is about 70 to 80. This heating ratio is relatively unchanged by placing various filters between the device and the oralloy. When a "fission" spectrum is used as a neutron source, the largest ratio is obtained when the oralloy heating is the smallest or when a layer of heavy material, such as tungsten, is placed just below the oralloy. The heavy material reduces the number of high-energy neutrons by converting them into neutrons of lower energy through nonelastic events. These lower energy neutrons produce fission in the oralloy but cannot generate inelastic gamma rays in the molybdenum, thus raising the heating ratio to $\sim$ 80. When the heavy material is placed halfway between the source and the oralloy, both the heating ratio and the total heating of the oralloy are drastically reduced.

The next problem which can be considered using MCNG is the uniformity of the heating of the oralloy across its surface. This problem arises since an essentially point source is being used in an attempt to generate a planar shock. From a device with a nominal yield of $\gtrsim 3$ kT (13 TJ), there are sufficient neutrons to allow the spectrum to be tailored both geometrically and spectrally by removing the unwanted ones with a filter.

With the goal of making the heating pulse rise time as fast as possible, calculations were performed with various thicknesses of polyethylene to remove the low-energy neutrons. This polyethylene filter was placed halfway between the source and the oralloy in order to provide the optimum solid angle for reducing the heating effect of the neutrons scattered by the filter. By making the polyethylene conically shaped, fewer neutrons would be removed from the edge of the beam than from the center. This compensated for the greater $1/r^2$-dependent heating of the center, as well as for less heating near the edge of the oralloy due to leakage effects. In order to decrease the leakage of moderated neutrons from the filter at late times, boron was added to the polyethylene. In addition to the boron-loaded polyethylene to shape the neutron spectrum, a layer of lead to remove some of the high-energy neutrons through nonelastic events was placed above the polyethylene. Besides removing high-energy neutrons,

the lead decreased the overall neutron flux without appreciably adding to the number of late-time, moderated neutrons. The top surface of the lead was spherically shaped in order to maintain uniform heating of the oralloy.

In addition to shaping the filter to provide uniform heating of the oralloy, leakage effects at its edges were decreased by surrounding the oralloy with uranium depleted in ^{235}U (D-38). The heating across the oralloy surface was maintained constant to about 5% by using a combination of the filter and the D-38, and the energy deposition reached about 85-90% of its maximum value in ∿ 0.1 μs (see Fig. 8).

B. Hydrodynamic Calculations Using Theoretical EOS

In order to predict shock strengths and subsequent histories, one-dimensional hydrodynamic calculations were performed using the code PAD.[11] These calculations were at first carried out by J. D. Jacobsen while a version of the code using the MAPLE and SESAME EOS libraries (computer files containing calculated EOS data in tabular form for various materials) was being debugged. Later calculations were performed using a version of the code which allowed for time-dependent energy deposition in the oralloy.

Figure 3 shows the calculated particle velocity for molybdenum layers 1 mm apart starting at the interface between a 10-mm-thick oralloy slab and a 15-mm-thick molybdenum slab. The total energy deposition in the oralloy and the rate were determined from the Monte Carlo calculations described in Sec. II-A. At approximately 0.7 μs the rarefaction from the surface of the oralloy nearer the device catches the shock and initially causes a decrease in the particle velocity for some layers near this front surface, whereas for layers nearer the back surface, at about the same time, the rarefaction from the back surface of the preheated molybdenum causes an increase in the particle velocity.

If a foil were placed 3 mm into the molybdenum, the particle velocity at the foil would be constant from ∿ 0.3 μs to ∿ 0.8 μs. Thus neutrons passing during this time would see the resonances shifted in energy by an amount corresponding to a velocity of ∿ 11 mm/μs. However, neutrons arriving at the foil before 0.3 μs would see a stationary foil or one whose velocity was rapidly changing, and neutrons

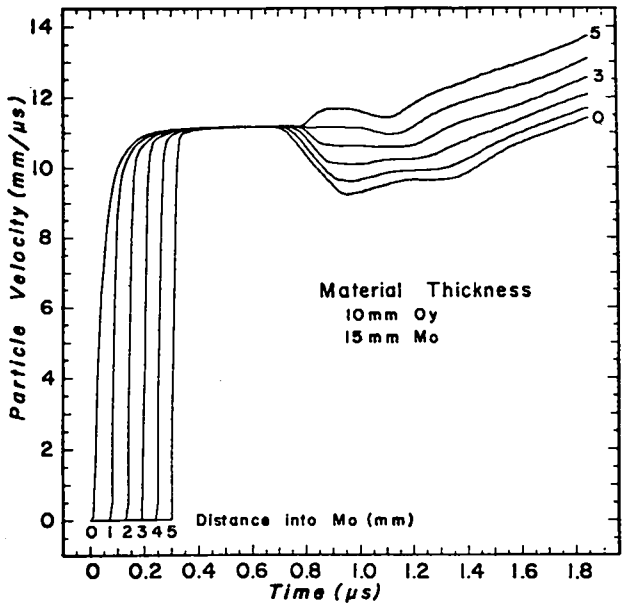

Fig. 3. Plot of the calculated particle velocity at several positions in a 15-mm slab of molybdenum when a 10-mm slab of oralloy is used as the driving material. Approximately 8 Terg/g are deposited in the oralloy while 0.1 Terg/g are deposited in the molybdenum, and the pressure behind the shock is 2.1 TPa. The finite rise times are due mainly to the rate of energy deposition in the oralloy. The velocity of the molybdenum near the oralloy is decreased, starting at about 0.7 μs, by the rarefaction propagating into the molybdenum from the oralloy. The layers of molybdenum near the back surface increase in velocity at approximately 0.8 μs because of the rarefaction from the back surface of the preheated molybdenum. These two effects approximately cancel for the layer at a depth of 4 mm into the molybdenum.

arriving after 0.8 μs would see a foil moving with a velocity of ∿ 10.5 mm/μs out to a time of about 1.2 μs. Thus a neutron source which produces most of the neutrons at the required resonance energy during the interval from 0.3 to 0.8 μs after the initial burst is needed. The most important requirement is that very few neutrons arrive after 0.8 μs.

Figure 4 shows a plot similar to Fig. 3, except that for this case a 14-mm-thick slab of oralloy with a 3-mm layer of $(CH)_n$ (e.g., Lucite) between it and the molybdenum is employed. The thicker oralloy prevents the rarefaction from the surface nearer the device from catching the shock, thus lowering the particle velocity. The structure

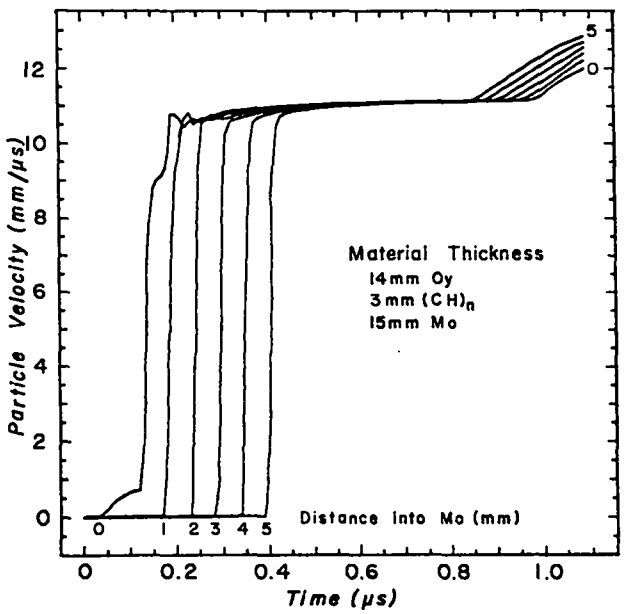

Fig. 4. Plot of the calculated particle velocity at several positions in a 15-mm-thick molybdenum slab. The driver is a 14-mm-thick oralloy slab with a 3-mm-thick slab of $(CH)_n$ between the oralloy and molybdenum. The total energy deposited in the oralloy was approximately 8 Terg/g and a pressure behind the shock of 2.1 TPa was generated. The structure in the particle velocity as a function of time is due to reflections across the $(CH)_n$ layer. The velocity of a layer 5-mm deep in the molybdenum is increased at approximately 0.85 μs when the rarefaction into the preheated molybdenum reaches the shock front. The rarefaction from the oralloy surface does not arrive in time to cause a decrease in velocity.

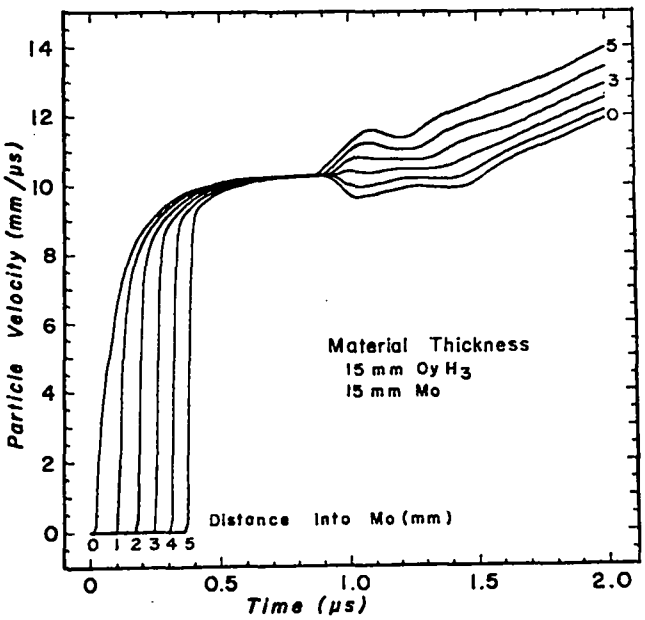

Fig. 5. Plot of the calculated particle velocity at several positions in a 15-mm-thick slab of molybdenum. The shock driver is, in this case, a 15-mm-thick slab of OyH_3. The rise time is much longer than in Figs. 3 and 4 because of the lower heating rate for the OyH_3. The rarefaction from the OyH_3 causes a drop in particle velocity at the front surface of the molybdenum at approximately 0.95 μs, and the rarefaction from the preheated molybdenum causes an increase in the particle velocity at a depth 5 mm into the molybdenum at approximately 0.9 μs. The particle velocity is approximately constant at the 3-mm position from 0.5 to 0.9 μs.

is due to reflections across the compressed layer of $(CH)_n$. The period during which the particle velocity is constant has now been shifted out to the time from 0.4 to 0.9 μs. This layer of $(CH)_n$ will, however, serve as a source of moderated neutrons. The next task is to determine the neutron spectrum from the $(CH)_n$ as a function of time. The nature of this spectrum will, to some extent, dictate the energies of the neutron resonances to be used to measure the particle velocity.

Since the density of the hydrogen in the moderating layer determines the time between neutron collisions with protons, and thus the moderation time, this parameter must be fed back into the Monte Carlo code to calculate the moderated neutron spectrum as a function of time. For the configuration shown in Fig. 4, the $(CH)_n$ is compressed in about 0.15 μs by a factor of 3 to 4; thus the moderation time of the neutrons is decreased by a factor of 3 to 4. The problem now is to determine what energy neutrons will emerge after about 0.4 μs.

Figure 5 shows plots of the particle velocity for various positions separated by 1 mm in a 15-mm molybdenum slab adjacent to a 15-mm-thick OyH_3 slab. The rise time of the shock is noticeably slower here, with a time of approximately 0.5 μs being required before neutrons should pass through a foil at 3 mm into the molybdenum. Figure 6 shows plots of the

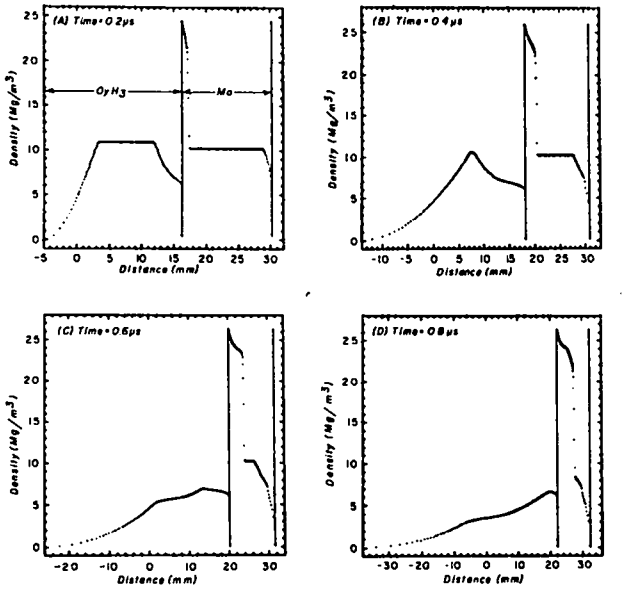

Fig. 6. Plots of the density in a 15-mm-thick slab of OyH_3 and a 15-mm-thick slab of molybdenum at times of 0.2, 0.4, 0.6, and 0.8 μs after the initial neutron burst. At t = 0 the densities were 10.92 Mg/m^3 for the OyH_3 and 10.2 Mg/m^3 for the molybdenum. At 0.2 μs most of each material is still at the initial density. At later times the density of the OyH_3 decreases as a rarefaction propagates inward from the left and a shock is driven into the molybdenum at the right. The effect of the preheated molybdenum can be seen as a rarefaction moves inward from the right.

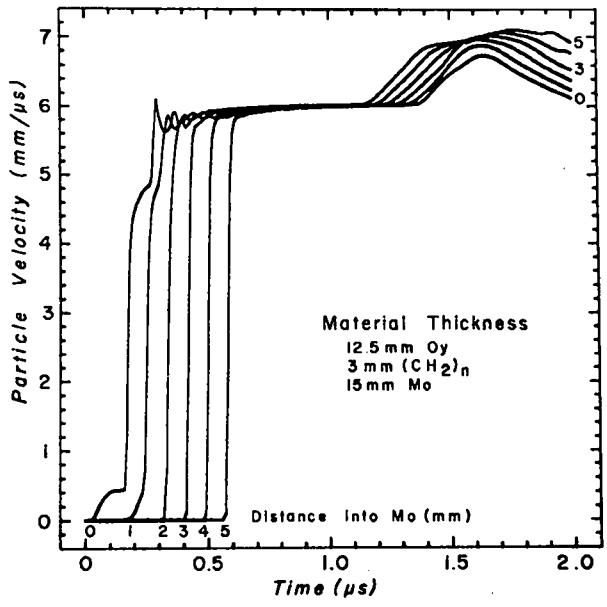

Fig. 7. Plot of the particle velocity at several positions in a 15-mm-thick slab of molybdenum. The driver is a 12.5-mm slab of oralloy with a 3-mm slab of $(CH_2)_n$ between the oralloy and molybdenum. The total energy deposited in the oralloy was approximately 2.5 Terg/g and a shock pressure of approximately 0.8 TPa was generated. The structure in the particle velocity as a function of time is due to reflections across the compressed $(CH_2)_n$ layer. The velocity at a position 5 mm into the molybdenum is increased at approximately 1.3 μs when the rarefaction from the preheated molybdenum reaches the shock front. This velocity is then decreased at approximately 1.6 μs when the rarefaction from the free surface of the oralloy reaches a given position in the molybdenum.

density profile for this configuration at times of 0.2, 0.4, 0.6, and 0.8 μs after the initial burst of neutrons. The density of the OyH_3 is seen to be decreasing, thus increasing the moderation time and increasing the amount of late time heating from moderated neutrons. The one nice feature of the OyH_3 is the fact that it serves as both a driver and a moderator. Thus there are no reflections across a compressed moderator.

For a shock pressure of 0.8 TPa the corresponding particle velocity in molybdenum is ∿ 6 mm/μs. The plots of the particle velocities at various distances into the molybdenum are shown in Fig. 7 for this experiment. The molybdenum slab is 15-mm thick with an oralloy driver 12.5-mm thick and with a 3-mm-thick layer of CH_2 between the two. For a position 3 mm into the molybdenum, a time of 0.5 μs is required for the particle velocity to reach 95% of 6 mm/μs, but this velocity remains constant until approximately 1.3 μs. Thus the time during which the particle velocity is constant is longer, but this value is not reached until a later time. Therefore, the moderated neutrons must not reach a foil at this position until after 0.5 μs.

All of the calculations in this section are based on the information that is being sought, namely, the molybdenum EOS. The calculated particle velocities using different equations of state[12] vary by as much as 10%, but the time during which the particle velocity is constant has even less variation. Thus the optimum times during which the moderated neutrons should pass through the molybdenum are rather insensitive to the theoretical molybdenum EOS. However, the overall calculations are sensitive to the density of the compressed moderator since this

determines the times at which the low-energy neutrons are produced.

C. Moderated Neutron Spectra

The number of moderated neutrons as a function of time was calculated using the code MCNG,[10] with feedback about the density of the moderator coming from the hydrodynamic calculations.[11] Twenty to thirty minutes of CDC 7600 time were required in order to obtain adequate statistics (30%) on the number of low-energy neutrons emerging from the moderator.

Calculations were performed using $(CH_2)_n$ and $(CH)_n$ moderators at densities ranging from 1.0 to 3.5 times the natural density. As expected, more moderated neutrons were produced by a given thickness of $(CH_2)_n$ than by $(CH)_n$, but at a density of 3.5 times the natural density, the neutrons from $(CH_2)_n$ were produced too early in time to be suitable for measuring U_p. Calculations were also performed using OyH_3 as a moderator. Since the OyH_3 expands as it drives a shock into the molybdenum, the 3-mm layer of OyH_3 nearest the molybdenum was assumed to have half the natural density; thus low-energy neutrons were still being produced at late times.

Based on its overall performance, the OyH_3 is not as favorable as the oralloy plus moderator for these experiments.

In order to observe the Doppler shifts of the neutron resonances, a TOF system with a flight path of 25 m was designed. The neutron spectrum was observed at 25 m by using a 10-mg/cm^2 ^{6}LiF deposit on a stainless steel backing in conjunction with three silicon solid-state detectors, connected in parallel to enhance the signal. The reaction products from ^{6}Li(n,α)t interacted with the diffused-junction detectors to produce currents proportional to the instantaneous neutron flux, which contained the resonance structure of interest.

Figure 8 shows a schematic of the 2.1-TPa experiment and Table I gives the calculated number of neutrons below 500 eV crossing a surface 5 mm into the molybdenum in the upward direction. If the foil employed to measure the particle velocity is located in this plane, then the neutrons arriving before 0.2 μs will pass through and heat a stationary foil. These neutrons will provide a signal that

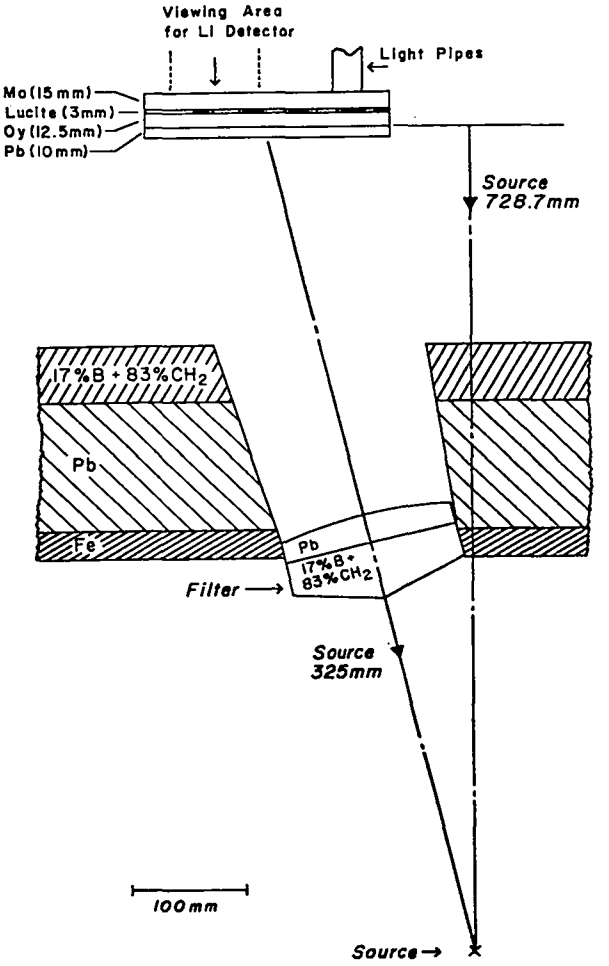

Fig. 8. Schematic of the setup for the 2.1-TPa experiment. The filter of lead and boron-loaded polyethylene was placed in a hole through 114 mm of lead and 50.8 mm of boron-loaded polyethylene. These materials were used to shield the oralloy from unwanted direct neutrons. The oralloy slab was surrounded by a ring of D-38 to decrease leakage effects from the edge of the oralloy. The Lucite served as a source of moderated neutrons, and when compressed by a factor of ∿ 3.5 provided a neutron pulse with a width of ∿ 0.5 μs for 20-50 eV neutrons.

TABLE I

NEUTRONS CROSSING A SURFACE 5 mm INTO MOLYBDENUM
(x 10^{-8}/SOURCE NEUTRON)

Time (μs)	Energy (eV) 1-5	5-10	10-20	20-50	50-100	100-200	200-500
0.0-0.2	---	---	---	1.9	2.7	4.2	25.3
0.2-0.3	---	1.5	2.5	2.4	2.0	7.1	5.5
0.3-0.9	1.8	2.8	4.4	5.0	4.1	8.2	26.1
0.9-2.0	---	4.3	1.4	2.0	7.1	7.1	42.5

shows unshifted resonances, as well as producing a background at the positions of the shifted resonances. The neutrons arriving between 0.2 and 0.3 μs will pass through a foil whose velocity is changing rapidly. Those neutrons arriving between 0.3 and 0.9 μs will pass through a foil moving with the particle velocity U_p (≈ 11 mm/μs). These neutrons will produce a signal at the detector that shows a dip at the shifted resonance position and a background at the unshifted resonance position. The neutrons arriving after 0.9 μs will pass through a foil whose velocity is changing, but hopefully the signal from these neutrons will be small. From Table I the energy intervals from 10-20 eV and 20-50 eV appear to be the best for obtaining a large number of neutrons between 0.3 and 0.9 μs and a small number of neutrons before and after this interval. Since it is desirable to keep the embedded foil thin in order to avoid hydrodynamic problems, the foil material should have one or more large resonances in this energy interval

Figure 9 shows a schematic of the part of the 0.8-TPa experiment above a boron-loaded polyethylene and lead filter which is similar to the one in Fig. 8. The oralloy driver in this case is adjacent to the molybdenum and the 7.5-mm $(CH_2)_n$ moderator is placed 40 mm below the oralloy. The auxiliary 3-mm slab of oralloy is placed below the moderator in order to decrease the pulse width of the moderated neutrons by compressing the $(CH_2)_n$ (by a factor of ∿ 2.7). When a moderator of $(CH)_n$ is placed between the oralloy and the molybdenum, the compressed $(CH)_n$ produces too many early time neutrons (before 0.5 μs). However, by placing the moderator some distance below the embedded foil, this narrow pulse of neutrons is delayed in arrival by time of flight. The price that is paid for this method of timing is a severe attenuation of the low-energy neutron flux by absorption in the oralloy driver. For this reason, a 10-mm slab of oralloy was used instead of a 12.5-mm slab. Table II gives the moderated neutron flux below 500 eV passing through the front surface of the molybdenum in the upward direction as a function of time. Note that there are virtually no neutrons below 50 eV because of absorption by the oralloy at low energy. Therefore, for this geometry, a foil material with one or more resonances with energies between 50 and 200 eV is needed.

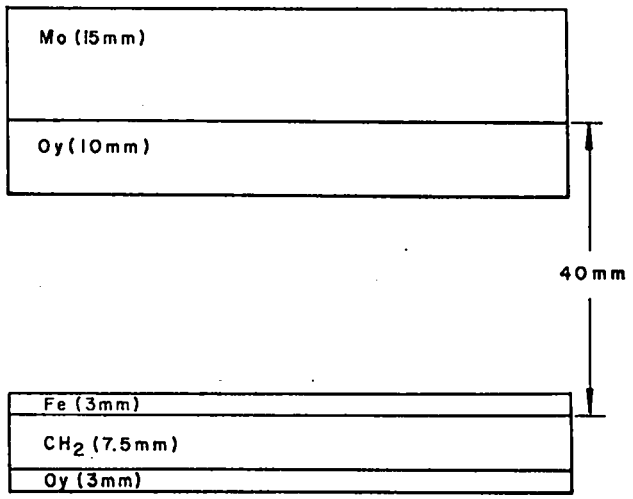

Fig. 9. Schematic of the part of the 0.8-TPa experiment above the lead and boron-loaded polyethylene filter. This filter is similar to the one shown in Fig. 8. The oralloy driver for this experiment is adjacent to the molybdenum and only 10-mm thick. This thickness allows better transmission of the slow neutrons moderated in the 7.5-mm compressed $(CH_2)_n$ layer placed 40 mm below the molybdenum. There are essentially no neutrons below 50 eV transmitted through the oralloy, and the pulse width of the 100-200-eV neutrons is approximately 0.4 μs. The 3-mm oralloy and iron layers maintain a compression of a factor of about 2.7 in the $(CH_2)_n$ for most of this time.

TABLE II

NEUTRONS CROSSING THE FRONT SURFACE OF MOLYBDENUM

($\times 10^{-8}$/SOURCE NEUTRON)

Time (μs)	Energy (eV) 1-5	5-10	10-20	20-50	50-100	100-200	200-500
0.0-0.2	---	---	---	---	---	---	---
0.2-0.5	---	---	---	---	---	2.0	4.0
0.5-1.3	---	---	---	0.3	1.6	2.0	1.0
1.3-3.0	---	---	---	---	---	0.1	0.3

D. Calculation of Expected Structure in the Low-Energy Neutron Flux

Figure 10 shows the total cross section of molybdenum[13] in the 0-200 eV energy interval. Indicator foil resonances are excluded for the regions around 12 and 45 eV for the 2.1-TPa experiment, and the regions around 71, 131, and 160 eV are excluded for the 0.8-TPa experiment because of the molybdenum resonances. The exact excluded regions will depend

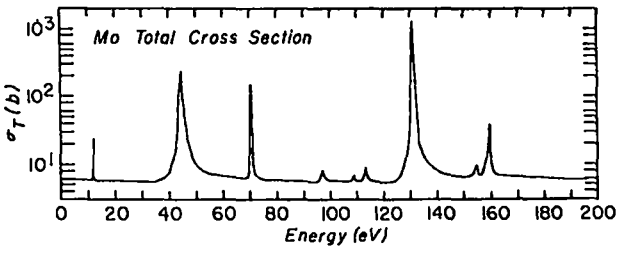

Fig. 10. Plot of the molybdenum total cross section from Ref. 13, with prominent resonances at 12.1, 45.1, 70.93, 131.4, and 159.5 eV.

on the Doppler widths of the resonances, the shift caused by the particle velocity, and the transmission of the 15-mm-thick molybdenum slab. These details are discussed below.

For widely spaced resonances the single-level Breit-Wigner formula may be used to represent the cross section. For low-energy neutrons (<< 1 keV) the total cross section in barns for a single isotope j may be expressed as[14]

$$\sigma_j = 4\pi a_j^2 + \frac{6.52\times10^5}{\sqrt{E}}\left[\frac{\Gamma g\Gamma_n^o}{(\Gamma/2)^2+(E_o-E)^2}\right] - 5.725\times10^3\left[\frac{(E_o-E)g\,\Gamma_n^o a_j}{(\Gamma/2)^2+(E_o-E)^2}\right], \quad (1)$$

where E is the neutron energy relative to the nucleus in eV, $\Gamma_n = \Gamma_n^o\sqrt{E}$, g is the statistical weight factor, and a_j represents the potential scattering amplitude. For the case where several isotopes with fraction $f_j(\Sigma f_j = 1)$ are present and several resonances may contribute to the cross section, let

E^λ = resonant energy of resonance λ,
Γ^λ = total width of resonance λ,
$\Gamma_n^{o\lambda}$ = reduced neutron width of resonance λ,
f^λ = fractional abundance of isotope which contains resonance λ,
g^λ = statistical weight,
r = nuclear radius,
a = potential scattering amplitude.

Then

$$\sigma(E'') = 4\pi r^2 + \frac{6.52\times10^5}{\sqrt{E''}}\sum_\lambda \frac{\Gamma^\lambda\left(fg\Gamma_n^o\right)^\lambda}{(E^\lambda-E'')^2+(\Gamma^\lambda/2)^2} - 5.725\times10^3\sum_\lambda \frac{\left(E^\lambda-E''\right)\left(fg\Gamma_n^o\right)^\lambda a}{(E^\lambda-E'')^2+(\Gamma^\lambda/2)^2}. \quad (2)$$

This expression includes interference between the resonance and the potential scattering, but not between resonances.

The Doppler-broadened cross section can be calculated by convoluting the cross section of Eq. (2) with a Doppler function. For the case in which the random Maxwellian velocity of the nucleus is much less than the neutron velocity, the Doppler function can be well approximated by a Gaussian with a 1/e width $\Delta = 2(mE_rkT/M)^{1/2}$, where m is the neutron mass, M is the mass of the nucleus, and T is the temperature. The broadened cross section thus becomes

$$\sigma_\Delta(E') = \frac{1}{\Delta\sqrt{\pi}}\int_o^\infty \sigma(E'')\exp\left[-\left(\frac{E'-E''}{\Delta}\right)^2\right]dE'' \quad (3)$$

This integral can be evaluated in terms of the real and imaginary parts of the complex probability integral

$$W(Z) = \frac{1}{\pi}\int_{-\infty}^{\infty}\frac{\eta^\lambda\, e^{-S^2}}{\left(\xi^\lambda-S\right)^2+\left(\eta^\lambda\right)^2}\,dS + \frac{i}{\pi}\int_{-\infty}^{\infty}\frac{(\xi^\lambda-S)\, e^{-S^2}}{\left(\xi^\lambda-S\right)^2+\left(\eta^\lambda\right)^2}\,dS, \quad (4)$$

where

$$\eta^\lambda = \frac{\Gamma^\lambda/2}{\Delta}, \quad \xi^\lambda = \frac{(E^\lambda-E')}{\Delta}, \quad \text{and} \quad S = \frac{(E''-E')}{\Delta}.$$

Substituting Eq. (2) into Eq. (3) and letting $U(\xi^\lambda,\eta^\lambda)$ and $V(\xi^\lambda,\eta^\lambda)$ represent the real and imaginary parts of W(Z), respectively, gives

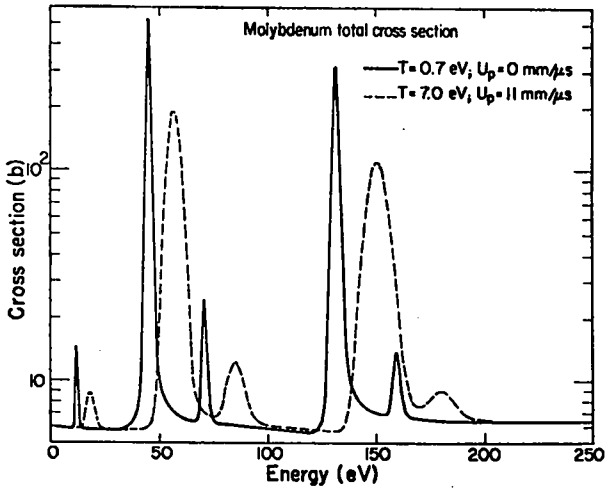

Fig. 11. Plot of the apparent molybdenum cross section at temperatures of 0.7 eV (solid curve) and 7.0 eV (dashed curve). The 7.0-eV cross section was calculated assuming a particle or mass velocity of 11 mm/μs in order to show the Doppler shift at this velocity. These plots were made using the code described in Sec. II-D. The 70.93-eV resonance should provide a measure of the molybdenum preheat and of the "average" particle velocity behind the shock.

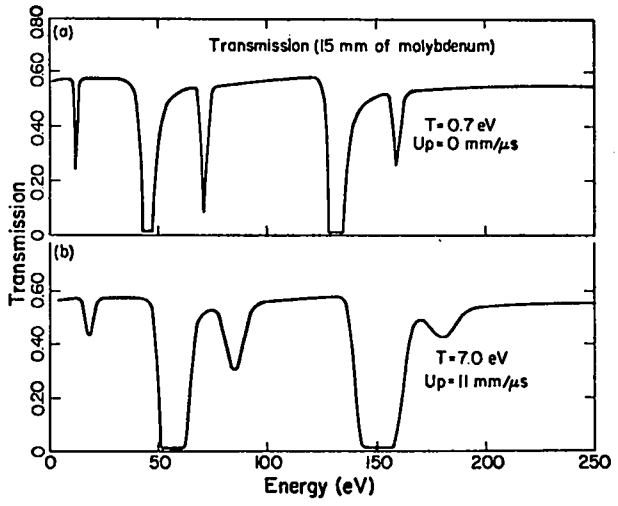

Fig. 12. Plots of the calculated transmission of a 15-mm-thick molybdenum slab for the cross sections shown in Fig. 11. Part (a) shows the transmission at a temperature of 0.7 eV and at a particle velocity of 0 mm/μs. Part (b) shows the transmission at a temperature of 7.0 eV and at a particle velocity of 11 mm/μs. The regions free of molybdenum resonances are: < 12 eV, 20-40 eV, 95-125 eV, and > 185 eV.

$$\sigma_\Delta(E') = 4\pi r^2 + \frac{2\sqrt{\pi}}{\Delta} \sum_\lambda \left(\ell g \Gamma_n^o\right)^2 \left\{ 6.52\times10^5 \left[\frac{1}{\sqrt{E'}} - \frac{\Delta\xi^\lambda}{2(E')^{3/2}} \right] U\,(\xi^\lambda, \eta^\lambda) \right.$$

$$\left. + \left[6.52\times10^5 \frac{\Delta\eta^\lambda}{2(E')^{3/2}} - 2.8625 \times 10^3\, a \right] V(\xi^\lambda\, \eta^\lambda) \right\} \quad . \qquad (5)$$

The transmission as a function of neutron energy, for a given thickness of material, can then be computed from this cross section and the resonance parameters in Ref. 13.

Figure 11 shows a plot of the apparent molybdenum total cross section at temperatures of 0.7 and 7.0 eV in the energy interval 0-200 eV. The cross section at T = 7.0 eV has been calculated assuming a particle velocity of 11 mm/μs. The resonance parameters are from Ref. 13 with the exception of those from the paper by Shwe and Coté[15] for the p-wave resonance at 12.1 eV.

In calculating the cross section for a moving material at a given neutron energy, the velocity of the neutron relative to the material is used to compute the energy to be used in Eqs. (4) and (5). The transmission of a 15-mm-thick slab of molybdenum is given in Fig. 12 for the cross section of Fig. 11. The region below ∿ 38 eV is not complicated by molybdenum resonances except for dips around 12 and 20 eV. The region from 95 to 125 eV is also uncontaminated, as well as the region above ∿ 185 eV.

The size of all of these dips in the signal will depend upon the thickness of the material ahead of and behind the shock. For the 12-eV resonance, for example, most of the molybdenum will be behind the shock when the neutrons are produced, and the unshifted dip will be very small.

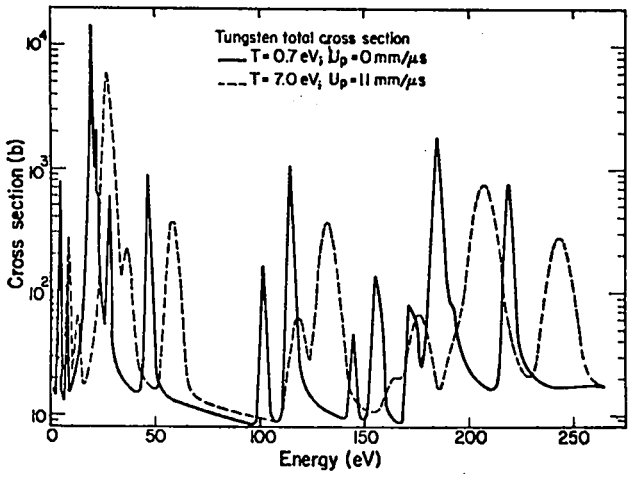

Fig. 13. Plot of the apparent cross section for natural tungsten at temperatures of 0.7 eV (solid curve) and 7.0 eV (dashed curve). The 7.0-eV curve was calculated at an assumed particle velocity of 11 mm/μs. The 18.84-eV resonance is shifted up to an energy of 26.4 eV and lies on top of the 27.13-eV resonance. However, the cross section of the 18.84-eV resonance is still a factor of 10 larger than that of the 27.13-eV resonance. The 21.2-eV resonance causes only a minor perturbation in the shape of the 18.84-eV resonance. The 114-eV resonance is not suitable for measuring the particle velocity because the shifted resonance (132 eV) is obscured by the 131.4-eV molybdenum resonance. The 184.6- and 219.0-eV resonances appear to be suitable for use in the 0.8-TPa experiment.

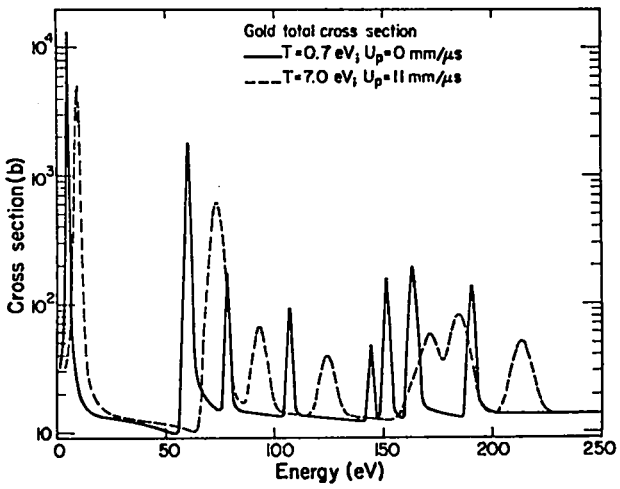

Fig. 14. Plot of the gold apparent total cross section calculated at temperatures of 0.7 and 7.0 eV. The 7.0-eV cross section was calculated assuming a particle velocity of 11 mm/μs. The 4.906-eV resonance would be useful in the energy range below 12 eV, and for a thin foil (25 μm) the 60.25-eV resonance should not interfere with the 70.93-eV molybdenum resonance.

Tungsten and gold will now be considered for use as the indicator foil. Figure 13 shows the total cross section for natural tungsten at temperatures of 0.7 and 7.0 eV, with a particle velocity of 11 mm/μs being assumed for the 7.0-eV calculation. Figure 14 shows the total cross section for gold at 0.7 and 7.0 eV, with the 7.0-eV calculation being performed at a particle velocity of 11 mm/μs.

The 4.9-eV resonance in gold shifts up to 9.0 eV at a particle velocity of 11 mm/μs and should not interfere with the rather small expected dip from the 12-eV molybdenum resonance. The 18.84-eV resonance in the tungsten is about a factor of eight larger than the nearby 21.2-eV resonance, and the smaller resonance should not appreciably distort the larger one in the final signal. These 4.9-eV gold and 18.84-eV tungsten resonances appear to be rather well suited for measuring the particle velocity in the 2.1-TPa experiment. Since the peak cross section for the 18.84-eV resonance at a temperature of 7.0 eV is approximately 6000 b, a 25-μm tungsten foil would provide about 40% transmission. The gold has a similar cross section and a 25-μm foil would provide a similar transmission. The 60-eV gold resonance at a temperature of 7.0 eV should produce no more than a 5% dip in the signal. Thus, the energy region around 70-90 eV should be relatively clean except for the 70.93-eV molybdenum resonance. The width of this resonance should allow the preheat temperature to be determined, and the shift should provide information on the "average" particle velocity behind the shock.

The 184.6-eV tungsten resonance appears to be suitable for determining the particle velocity in the 0.8-TPa experiment. The resonances at 182.4 and 219.0 eV should cause no appreciable distortion of the 184.6 resonance. Since the peak cross section for this resonance is approximately 700 b at a temperature of 7.0 eV, a 177.8-μm foil would provide about 45% transmission. The 70.93-eV molybdenum resonance will provide for the 0.8-TPa experiment a measure of the preheat temperature, as well as information on the average particle velocity behind the shock.

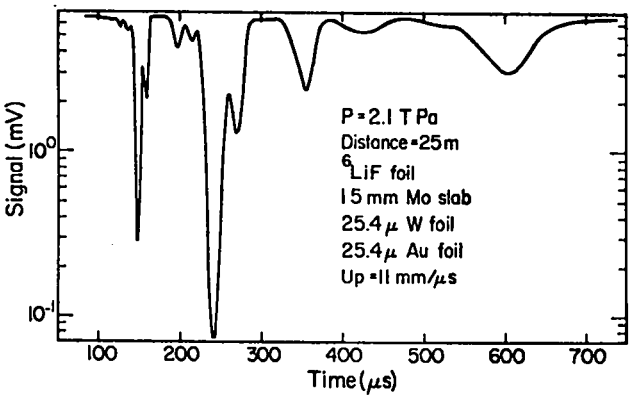

Fig. 15. Plot of the expected signal as a function of time for the 2.1-TPa experiment, using a ^{6}LiF foil at a distance of 25 m. The arrival times of the neutrons corresponding to the prominent resonances are given in Table III. The average apparent off-resonance signal level should be larger at the early time, but for calculational ease it was assumed to be constant. The dip at 350 μs corresponds to the shifted 18.84-eV tungsten resonance, and the dip at 600 μs corresponds to the shifted 4.906-eV gold resonance. The locations of these two dips allow a determination of the particle velocity. The width of the dip at approximately 210 μs (70.93-eV molybdenum resonance) should allow the preheat temperature of the molybdenum to be determined. The doublets at 150 to 160 μs and at 240 to 270 μs correspond to the shifted and unshifted 131.4- and 45.1-eV molybdenum resonances, respectively.

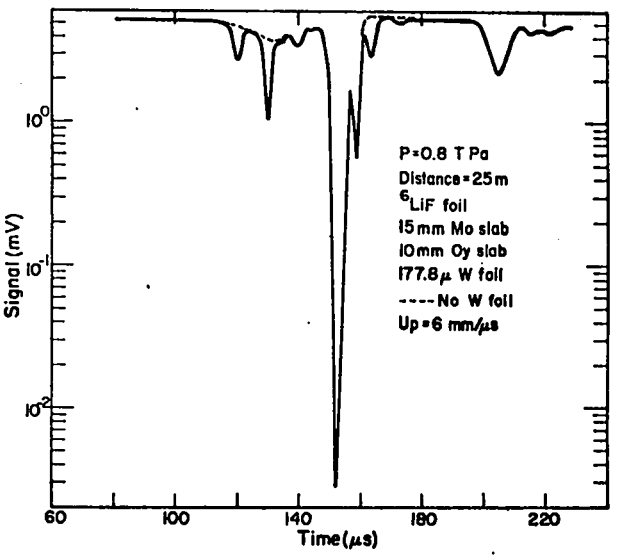

Fig. 16. Plot of the expected signal as a function of time for the 0.8-TPa experiment using a ^{6}LiF foil at a distance of 25 m. The arrival times of the various energy neutrons are given in Table IV. The dashed line shows the expected signal with no tungsten foil, but includes the effects of the 10-mm slab of oralloy (6.5% ^{238}U) as does the solid line. The large doublet at ∿ 150 μs corresponds to the 131.4-eV molybdenum resonance. The position of the dip at ∿ 130 μs (184.6-eV tungsten resonance) allows the determination of the particle velocity which, for this calculation, was assumed to be 6.0 mm/μs.

The number of neutrons of a given energy passing through the molybdenum and the indicator foil at a certain time can be used in conjunction with the shock position, the temperature ahead of and behind the shock, and the Doppler-broadened cross sections to calculate the expected signal level from the solid-state detectors.

For a geometry in which a 45-cm^2 area of molybdenum is viewed at 25 m by a 25-mm-diam spot on the ^{6}LiF foil, for a source strength of 10^{24} neutrons, and for a detector solid angle equal to 3% of a sphere, the approximate expected signal in mV into 50 Ω is given in Figs. 15 and 16 for the 2.1- and 0.8-TPa experiments, respectively. The average signals should actually decrease (because of a decrease in the number of moderated neutrons with energy) by about a factor of three in going from 80 to 650 μs, but this effect has not been included.

For the 2.1-TPa experiment (Fig. 15) the large dips at 148 and 241 μs are due to the 131.4- and 45.1-eV resonances in the molybdenum shifted by a particle velocity of 11 mm/μs. The smaller dips at 158 and 270 μs correspond to the same resonances at the unshifted energy and are smaller because most of the neutrons at these energies pass through material that is behind the shock front. Table III gives the calculated flight times of the larger shifted (U_p = 11 mm/μs) and unshifted resonances in the molybdenum, tungsten, and gold.

For the 0.8-TPa experiment the large dip in Fig. 16 at 152 μs is due to the 131.4-eV molybdenum resonance shifted by a particle velocity of 6 mm/μs, and the smaller dip at 158 μs is due to the unshifted 131.4-eV resonance in molybdenum. Table IV gives the positions of the larger resonances for this experiment. These calculations include the effect of the

TABLE III

RESONANCE NEUTRON FLIGHT TIMES FOR
2.1-TPa EXPERIMENT AT 25 m

Flight Time (μs)	Material	E_o (eV)	U_p (Assumed) (mm/μs)
600.0	Au	4.91	11
519.7	Mo	12.1	0
423.0	Mo	12.1	11
416.5	W	18.84	0
392.6	W	21.20	0
352.0	W	18.84	11
334.8	W	21.20	11
269.2	Mo	45.1	0
240.7	Mo	45.1	11
214.6	Mo	70.93	0
196.1	Mo	70.93	11
169.0	W	114.4	0
157.7	Mo	131.4	0
157.3	W	114.4	11
147.5	Mo	131.4	11
143.1	Mo	159.5	0
134.7	Mo	159.5	11
133.0	W	184.6	0
125.6	W	184.6	11

TABLE IV

RESONANCE NEUTRON FLIGHT TIMES FOR
0.8-TPa EXPERIMENT AT 25 m

Flight Time (μs)	Material	E_o (eV)	U_p (Assumed) (mm/μs)
214.6	Mo	70.93	0
204.1	Mo	70.93	6
179.6	W	101.3	0
172.2	W	101.3	6
169.0	W	114.5	0
162.4	W	114.5	6
157.7	Mo	131.4	0
151.9	Mo	131.4	6
143.1	Mo	159.5	0
138.4	Mo	159.5	6
133.0	W	184.6	0
131.3	^{238}U	189.6	0
128.9	W	184.6	6
122.2	W	219.0	0
118.7	W	219.0	6

10-mm oralloy driver between the moderator and the foil, and the dashed line in Fig. 16 shows the effect of removing the tungsten foil. The dip in the dashed line at 131 μs is due to the 189.6-eV resonance from the 6.5% ^{238}U in the oralloy, while the large dip in the solid line at 129 μs is due to the shifted 184.6-eV tungsten resonance.

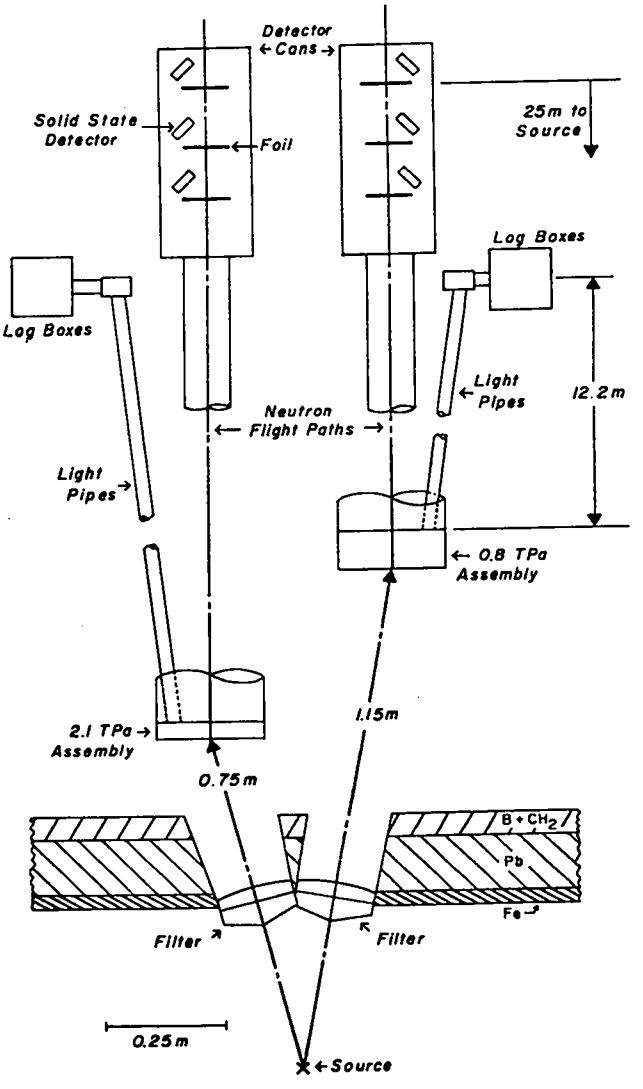

Fig. 17. Schematic of the overall layout for the two high-pressure experiments. The bottoms of the oralloy drivers for both the 2.1- and 0.8-TPa experiments were placed at distances of 0.75 m and 1.15 m from the device, respectively. The log boxes were placed 12.2 m from the molybdenum surfaces. Each foil in the detector cans was viewed by three solid-state detectors connected in parallel to enhance the signal. These detector cans were placed at a distance of about 25 m from the source for the two experiments.

III. CONCLUSIONS

For an underground shot at NTS in the fall of 1973 the neutron detectors for the two high-pressure experiments were placed in vacuum chambers at a distance of 25 m from the molybdenum sample. Figure 17 shows a schematic of the overall layout for these experiments. For the 2.1-TPa experiment, the detectors consisted of two ^{6}LiF foils (one for a backup) and a blank stainless steel foil to measure the background. For the 0.8-TPa experiment the detectors consisted of a ^{6}LiF foil, a blank stainless steel foil, and a deposit of 500 $\mu g/cm^2$ of $^{239}PuO_2$ on a 2.5-μm stainless steel backing. In both experiments each foil was viewed by three solid-state detectors connected in parallel to increase the effective solid angle for particle detection. The purpose of the plutonium foil was to provide a large signal at the peaks of fission resonances and thus a measure of the neutron flux at these energies if the flux was too small to produce a detectable signal from the ^{6}Li.

The signals from both experiments were dominated by large backgrounds and were saturated for at least 100 μs. The ^{6}Li signal from the 0.8-TPa experiment was lost completely because the amplifier for that signal burned out. One ^{6}Li signal for the 2.1-TPa experiment did not recover from saturation for approximately 600 μs. The other ^{6}Li signal recovered at approximately 150 μs, but the signal was still dominated by background. The signal from the plutonium foil did contain resonances as expected. From the areas and positions of the resonances, however, it was determined that the source of low-energy neutrons was about a factor of ten larger than expected and was displaced downward from the position of the expected source by about 350 mm.

On the shot the direct neutron flux to the high-pressure driver was collimated by a hole in 114 mm of lead and 51 mm of boron-loaded polyethylene (see Fig. 17). This collimating device was in the line of sight of the flux measurements, and the boron-loaded polyethylene acted as a source of moderated neutrons. This source was at the correct position to explain the anomalous source observed with the plutonium foil, and later Monte Carlo calculations indicated that the flux would be about an order of magnitude larger than the flux from the proper moderator. The signal from the plutonium foil also contained resonances at times corresponding to neutrons from the proper moderator. These resonances were approximately the size predicted by the preshot calculations.

These results don't suggest that any basic design changes are needed, but several important improvements in details should be incorporated in the next experiment. The large overall background from the solid-state detectors was produced by light from the line-of-sight pipe, and this background can be greatly reduced on future experiments by covering the detector chamber with a blank-off plate.

The measurements of the shock arrival times at three surfaces in the molybdenum were hampered by large backgrounds. These times were determined from the light flash emitted when the shock front reached a free surface using "log boxes" -- devices containing a set of three photomultipliers in conjunction with partially silvered mirrors to give approximately logarithmic response. The light was transmitted by polished pipes to the log boxes located 12.2 m away. One log box on each experiment was covered with a black rubber gasket, and light flashes sent up the pipe by a xenon flash lamp before the shot indicated that there was no light leak. On the shot itself these background log boxes showed very large signals essentially identical to the other log box signals. One explanation for these spurious signals is that scattered neutrons from a nearby line-of-sight pipe produced gamma rays in the lead shot surrounding the log boxes, and these gamma rays caused the short air path (50 mm) in front of each log box to glow. In a similar experiment on a previous shot, in which there was no other nearby pipe for neutrons, the background signal was essentially zero. The effects of this problem should be greatly reduced by designing the experiment so that there are no nearby pipes and also by using better shielding.

ACKNOWLEDGMENTS

The author would like to thank R. G. Schrandt for his advice on the running of the Monte Carlo code and J. D. Jacobson for his help in performing the hydrodynamic calculations. The author would like to thank B. C. Diven for many helpful discussions about the design of the experiment. Thanks are extended to the following people for their help in performing the high-pressure experiment at the Nevada Test Site: J. M. Anaya, B. C. Diven, D. M. Drake, A. N. Ellis, A. Hemmendinger, G. A. Keyworth, E. E. Robinson, R. C. Rosul, E. R. Shunk, and M. G. Silbert. The author also would like to thank J Division for fielding the experiment.

REFERENCES

1. W. E. Deal, Jr., "Dynamic High-Pressure Techniques," in Modern Very High Pressure Techniques, R. H. Wentorf, Jr., Ed. (Butterworth and Co., Ltd., Washington, 1962) Chap. 11, p 200-227.

2. L. V. Al'tshuller, B. N. Moiseev, L. V. Popov, G. V. Simakov, and R. F. Trunin, "Relative Compressibility of Iron and Lead at Pressures of 31 to 34 Mbar," Sov. Phys. JETP 27, 420 (1968).

3. R. F. Trunin, M. A. Podurets, B. N. Moiseev, G. V. Simakov, and L. V. Popov, "Relative Compressibility of Copper, Cadmium, and Lead at High Pressures," Sov. Phys. JETP 29, 630 (1969).

4. M. A. Podurets, G. V. Simakov, R. F. Trunin, L. V. Popov, and B. N. Moiseev, "Compression of Water by Strong Shock Waves," Sov. Phys. JETP 35, 375 (1972).

5. R. F. Trunin, M. A. Podurets, G. V. Simakov, L. V. Popov, and B. N. Moiseev, "An Experimental Verification of the Thomas-Fermi Model for Metals under High Pressure," Sov. Phys. JETP 35, 550 (1972).

6. R. F. Trunin, G. V. Simakov, M. A. Podurets, B. N. Moiseyev, and L. V. Popov, "Dynamic Compressibility of Quartz and Quartzite at High Pressure," Earth Physics 1, 13 (1970).

7. W. J. Carter, S. P. Marsh, J. N. Fritz, and R. G. McQueen, "The Equation of State of Selected Materials for High Pressure References," Los Alamos Scientific Laboratory report LA-DC-9990 (1968); R. G. McQueen, S. P. Marsh, J. W. Taylor, J. N. Fritz, and W. J. Carter, "The Equation of State of Solids from Shock Wave Studies," in High Velocity Impact Phenomena, Edited by R. Kinslow (Academic Press, Inc., New York, 1970), p 293-417.

8. A. H. Jones, W. M. Isbell, and C. J. Maiden, "Measurement of the Very-High-Pressure Properties of Materials Using a Light-Gas Gun," J. Appl. Phys. 37, 3493 (1966); J. A. Morgan, Los Alamos Scientific Laboratory, private communication (1974).

9. C. E. Ragan III, unpublished work (1973).

10. E. D. Cashwell, J. R. Neergaard, W. M. Taylor, and G. D. Turner, "MCN: A Neutron Monte Carlo Code," Los Alamos Scientific Laboratory report LA-4751 (1972); E. D. Cashwell, J. R. Neergaard, C. J. Everett, R. G. Schrandt, W. M. Taylor, and G. D. Turner, "Monte Carlo Photon Codes: MCG and MCP," Los Alamos Scientific Laboratory report LA-5157-MS (1972); R. G. Schrandt, "MCNG - Running Instructions," Los Alamos Scientific Laboratory, private communication (1973).

11. W. Fickett and J. Jacobson, Los Alamos Scientific Laboratory, private communication (1973).

12. J. F. Barnes and G. T. Rood, Los Alamos Scientific Laboratory, private communication (1973).

13. Neutron Cross Sections, Brookhaven National Laboratory report BNL-325, Supp. 2 (1966).

14. S. E. Atta and J. A. Harvey, "Numerical Analysis of Neutron Resonances," Oak Ridge National Laboratory report ORNL-3205 (1962).

15. H. Shwe and R. E. Coté, "Neutron Resonances of Molybdenum Isotopes," Phys. Rev. 179, 1148 (1969).